Incident-beam effects in electron-stimulated Auger-electron diffraction

Y. Gao and Jianming Cao
Department of Physics and Astronomy, University of Rochester, Rochester, New York 14627-0011
(Received 1 October 1990)

We have examined incident-beam effects in electron-stimulated Auger-electron diffraction (AED) on a cleaved GaAs(110) surface. The results indicate that incident-beam diffraction is significant in an AED experiment, and that the dissipative nature of the incident beam in contributing to the Auger process must be accounted for. We have developed a qualitative model that describes the trend of the polar-angle dependence of the Auger intensity for both the incident and exit beams. In calculating the diffraction features, we used a zeroth-order approximation to simulate the dissipation of the incident beam, which is found to adequately describe the experimental data.

INTRODUCTION

A knowledge of atomic identities, positions, and bonding mechanism within the first 3–5 layers of a surface is essential for any quantitative microscopic understanding of surface phenomena. In a series of experiments, Chambers *et al.* demonstrated that electron-stimulated Auger-electron diffraction (AED) is a sensitive probe for examining surface structures.[1] Together with x-ray photoelectron diffraction (XPD), AED has been developed as an important technique for determining site symmetries, coordination numbers, bond directions, and short-range order in the surface and interface region.[1–3]

XPD and AED are based on the strong forward scattering of x-ray photoelectrons or Auger electrons of kinetic energy above several hundred eV by overlaying lattice atoms, and the scattering process produces enhanced intensities at exit angles corresponding to the directions connecting the emitting atom with overlying nearest- and next-nearest-neighbor atoms.[4] Since core-level and Auger peaks are element specific, observation of the directions in which their intensities are enhanced constitutes a probe of the short-range order around a particular element.

In electron-stimulated Auger-electron diffraction, both incident primary electrons and exit Auger electrons are subject to the same forward-scattering mechanism. One would expect that the observed AED distribution be the convolution of both the incident- and exit-electron diffraction. Previous studies of AED, however, showed that the angular distribution can be reasonably well described by a straightforward kinematical or single-scattering cluster formalism in which only the outgoing-beam scattering is included.[1] This rather surprising result was suggested as being due to the experimental geometry, which was such that the peaks associated with the incoming- and outgoing-beam forward scattering nearly overlap, causing the two effects to reinforce one another.[5] A comparison of XPD, AED, and medium-energy electron diffraction (MEED) on Ni(100) and Cu(100) also shows that the observed diffraction patterns are very similar and the inclusion of the incident-beam diffraction in the calculations does not improve the quality of the fit to the experimental data.[6] These results would seem to suggest that incident-beam effects were of minor significance in AED experiments. The geometry in these experiments, however, is such that the angle between the incident and exit beam is fixed, and both diffraction angles are changed when the sample is rotated. Independent observation of incident-beam diffraction is therefore difficult with such an experimental setup, and effects of incident-beam scattering in an Auger-electron-diffraction measurement remain an open question.

In this paper, we report on our recent study of incident-beam effects in Auger electron diffraction on cleaved GaAs(110). Our experimental apparatus allowed us to fix the exit angle of the Auger electrons and vary only the incident angle, therefore isolating the incident-beam diffraction effects. Our results indicate that the incident beam does have a diffraction pattern different from that of the exit beam and the diffraction of the incident beam affects the observed data in a significant way. Furthermore, the incident-beam diffraction emphasizes larger polar angles, which is complementary to the exit-beam diffraction.

This paper is organized as follows. First, we describe our experimental apparatus. We then report our results and compare them with the continuum limit. The calculation of the diffraction of incident beam and the comparison to that of the exit beam will be given thereafter.

EXPERIMENT

Our ultrahigh-vacuum (UHV) chamber has a base pressure of about 7×10^{-11} Torr. Auger-electron (AES) and x-ray-photoemission (XPS) spectroscopies, as well as sample-preparation devices, were implemented in the system for the work described here. A clean GaAs(110) surface was prepared by cleaving a single-crystal post *in situ*. This surface was chosen for the present study because its geometry is well understood and easy to prepare.[7,8] A primary-electron beam of 3 keV energy from a Leybold EQ-22 electron gun is focused to a 0.5-mm-diam spot at the surface, with a beam current of ~0.3 μA. The Ga

LMM and As *LMM* Auger spectra were measured with a Vacuum Generator ADES 500 energy analyzer mounted on a two-axis goniometer in pulse-counting mode. The analyzer has been modified to have a 3 mm cross-sectional diameter $\times 20$ mm length entrance collimating cylinder to improve the angular resolution, which was determined by observing low-energy electron diffraction (LEED) to have a full width at half maximum (FWHM) of 1.6°.

The geometry of the experiment is shown in Fig. 1, in which the two rotational degrees of freedom of the sample, and the one rotational degree of freedom of the analyzer in the horizontal plane are illustrated. These three rotation angles were adjusted separately or concurrently, depending on the actual experiment. The other rotational degree of freedom of the analyzer in the vertical plane (not shown in Fig. 1) was used to optimize sample alignment, but otherwise remained fixed while data were taken. The minimum angle between the electron beam and the analyzer is 39°, which sets the limits of the incident-beam polar scan with normal exit angle.

The orientation of the sample was determined by observing the LEED maximum at 100 eV electron energy. The actual spot size of the incident electron on the sample surface varies with the incident angle Θ_0, and the geometry ensures that at $\Theta_0 = 80°$ from the surface normal, the full spot can still be covered by the analyzer entrance aperture and no signal is lost. The surface geometry is defined as the following. If $\hat{\mathbf{x}}$ is along $[1\bar{1}0]$ and $\hat{\mathbf{y}}$ along [001] and the surface Ga atom is located at $(0,0,0)a$, then the As atom would be located at $(\sqrt{2}/4, 1/4, 0)a$ if there were no surface relaxation. Here $a = 5.65$ Å is the GaAs lattice constant.[9] The polar angle Θ_0 (Θ_1) is defined to be positive if the beam is in the opposite side of $\hat{\mathbf{x}}$ (or $\hat{\mathbf{y}}$) with respect to the surface normal.

In taking an angular scan, three energy positions were selected to define the background and deduce the peak intensity of the Auger spectrum. The selection of the three positions are illustrated in Fig. 2 for Ga *LMM*, which shows that the background for the peak at position 2 is assumed to be on the straight line between positions 1 and 3. This method substantially reduced the time for data acquisition to about 25 min per angular scan and minimized surface deterioration. Alternative ways of data acquisition by integration over the full spectrum shown in Fig. 2 were also tested and the results were identical compared with those obtained with three energy positions as presented in this paper.

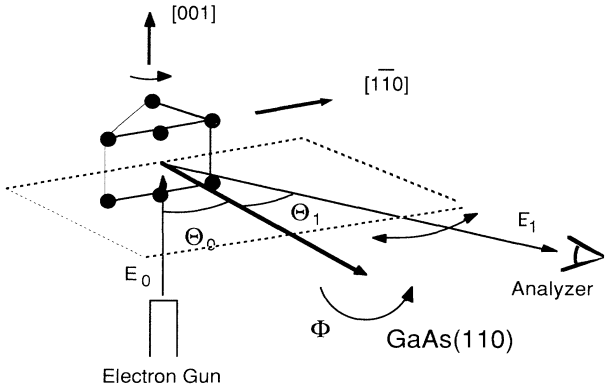

FIG. 1. The experimental geometry. The two degrees of freedom in rotation of the sample and the one degree of freedom in rotation of the analyzer being used in the experiments are marked.

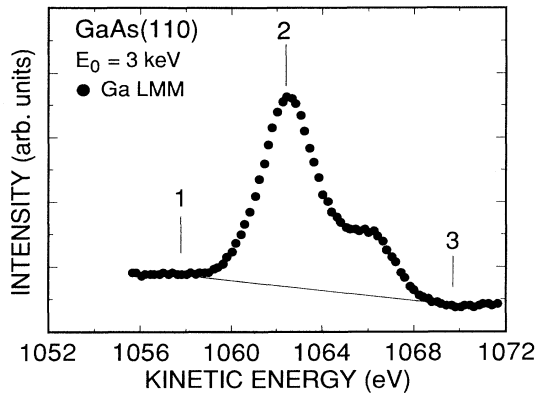

FIG. 2. A typical Ga *LMM* Auger spectrum from which three energy positions were selected for the angular scan. While positions 1 and 3 defined the background approximated as a straight line, the intensity of Ga *LMM* was taken as the peak height at position 2 from the background.

RESULTS AND DISCUSSION

Qualitative trend in the continuum limit

Figure 3(a) shows the Ga *LMM* Auger-electron-intensity dependence on the polar angle of a 3-keV

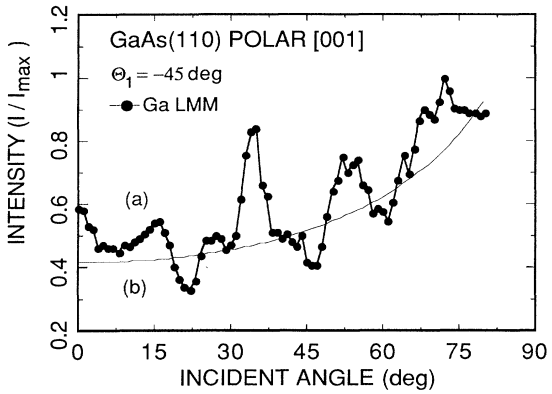

FIG. 3. (a) The incident-beam polar-angle scan of Ga *LMM* Auger intensity from GaAs(110) along [001]. The exit angle was kept at $\Theta_1 = -45°$. As the incident angle Θ_0 approaches the glancing angle at 90°, the intensity increases. (b) The results of the qualitative model at continuum limit, calculated using Eq. (3) with small correction of surface deflection.

incident-electron beam along the [001] direction of GaAs(110). The exit angle Θ_1 was fixed at $-45°$ by rotating both the sample and analyzer simultaneously. Scattering features can be clearly seen throughout the angular range. An interesting feature of the spectrum is the increase in Auger intensity as the incident angle approaches the glancing angle at $\Theta_0=90°$.

This trend is in sharp contrast to that of the exit-beam diffraction, shown in Fig. 4. The exit-beam diffraction data were taken by moving only the analyzer, while keeping the incident angle Θ_0 stationary at 80°. A scan was also taken along [001], but on the opposite side of the surface normal relative to that in Fig. 3. The exit-beam intensity clearly diminishes as the exit polar angle Θ_1 approaches the glancing angle at $-90°$.

The different behaviors of the incident- and exit-beam intensity at large polar angles can be understood on the basis of the different roles of these two beams. While the exit beam undergoes mostly elastic or nearly elastic scattering on its way out, the incident beam has to suffer a drastic inelastic scattering event to generate the Auger electron being observed. The increase in the Auger intensity when the incident beam approaches the glancing angle is therefore a result of more electrons dissipating energy near the surface region and creating more Auger electrons capable of escaping from the surface. This intuitive picture can be quantified in a continuum limit where the intensity of incident electrons inside the sample is described as

$$I=I_0 e^{-z/\lambda_0\cos\Theta_0}, \tag{1}$$

where I_0 is the incident intensity, λ_0 the electron inelastic scattering mean free path, and z the distance from the surface.

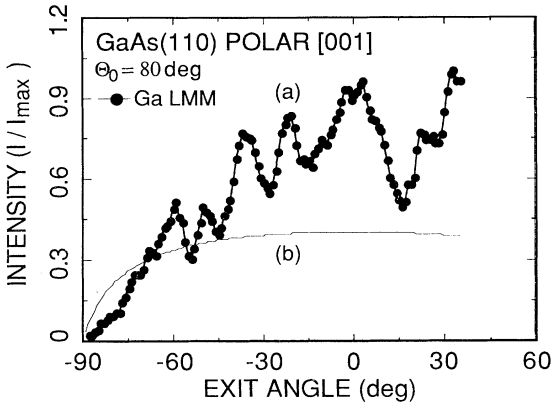

FIG. 4. (a) The exit-beam polar-angle scan of Ga *LMM* Auger intensity from GaAs(110) along [001]. The incident angle was kept at $\Theta_0=80°$. As the exit angle Θ_1 approaches the glancing angle at $-90°$, the intensity diminishes. (b) Results from the qualitative model in the continuum limit, calculated using Eq. (3) and small correction of surface deflection.

The number of Auger electrons excited in the layer between z and $z+dz$ is proportional to the dissipation of the incident beam in the same region,

$$i_{\mathrm{AE}}=-\alpha\frac{dI}{dz}=\frac{\alpha}{\lambda_0\cos\Theta_0}I_0 e^{-z/\lambda_0\cos\Theta_0}, \tag{2}$$

where α is the transition probability which, according to the Auger process, can be considered isotropic.[10,11] The measured Auger intensity at the exit angle Θ_1 can be obtained by integrating Eq. (2) with the attenuation of the outgoing Auger electrons incorporated:

$$I_{\mathrm{AE}}(\Theta_0,\Theta_1)=\int_0^\infty dz\, i_{\mathrm{AE}} e^{-z/\lambda_1\cos\Theta_1}=\int_0^\infty dz\frac{\alpha I_0}{\lambda_0\cos\Theta_0}\exp\left[-z\left[\frac{1}{\lambda_0\cos\Theta_0}+\frac{1}{\lambda_1\cos\Theta_1}\right]\right]$$
$$=\alpha I_0/(1+\lambda_0\cos\Theta_0/\lambda_1\cos\Theta_1). \tag{3}$$

Equation (3) indicates that for the constant exit angle Θ_1, the measured Auger intensity increases as Θ_0 increases, in qualitative agreement with our data in Fig. 3(a). A smooth curve using Eq. (3) with $\Theta_1=-45°$ and $\lambda_0/\lambda_1=[(3000\ \mathrm{kV})/(1000\ \mathrm{kV})]^{1/2}=1.432$ from the universal mean-free-path energy dependence,[12] together with a small correction for surface deflection, is presented in Fig. 3(b) and the qualitative agreement is demonstrated, except for structures due to diffraction. Using the same equation with $\Theta_0=80°$, we have also calculated Auger intensity as a function of the exit angles Θ_1. The resulting smooth curve is drawn in Fig. 4(b) and the reduction of the exit-beam intensity at large polar angles is reproduced. The calculated curves in Figs. 3(b) and 4(b) demonstrate that Eq. (3) qualitatively describes the polar-angle dependence of the Auger intensity of both the incident and exit beams in the continuum limit.

Calculation model of diffraction effects

The data shown in Figs. 3(a) and 4(a) clearly demonstrate that diffraction is important for both the incident primary electrons and outgoing Auger electrons. To calculate properly the diffraction features, one has to include the dissipation of the incident primary electrons at the site of the emitter and the elastic scattering of the outgoing Auger electron by the nearby atoms. Since the Auger process is an inelastic-scattering event in which the emitted Auger electrons have no memory of the phase of the incident-electron wave functions, the final result is the product of the above two parts times the Auger-process cross section without any phase correlations.[3,6] Furthermore, the inelastic nature of the Auger process dictates that Auger emissions are random events,

which excludes any phase relation between Auger excitations at different sites. One can therefore utilize the symmetry of the crystal and choose representative sites to simplify the calculations.

The angular dependence of elastic scattering can be well described by a kinematic or single-scattering model.[1-3] The outgoing Auger electron intensity for the lth emitter can be written as[6]

$$I_{\text{out}}^{(l)}(\mathbf{k}) \propto \left| \exp\left[\frac{-L_l}{2\lambda_1}\right] + \sum_j \frac{|f_j(\theta_j)|}{r_j} W_j \exp\left[-\frac{L_j + r_j}{2\lambda_1}\right] \exp\{i[|k| r_j(1-\cos\theta_j) + \psi_j(\theta_j)]\} \right|^2 + \sum_j \frac{|f_j(\theta_j)|^2}{r_j^2} \exp\left[-\frac{L_j + r_j}{\lambda_1}\right](1 - W_j^2) , \tag{4}$$

where $L_l = z_l / \cos\Theta_1$ is the path inside the solid of the unscattered, but attenuated wave $\exp(-L_l/2\lambda_1)$, r_j is the distance between the jth scatterer and the emitter, $f_j(\theta_j)$ is the scattering factor, and θ_j is the scattering angle from the jth scatterer. The phase changes due to path-length differences and scattering are incorporated in $|k| r_j(1-\cos\theta_j)$ and $\psi_j(\theta_j)$, respectively. Lattice vibrations are accounted for in the usual way by a Debye-Waller factor W_j, and the overcounting of the lattice vibration effects in the first summation over j is compensated by the last summation over j. Since only the first scattering of the outgoing wave is contained in Eq. (4), it can be termed as a single-scattering calculation. Another approximation in Eq. (4) is using the asymptotic form of the Auger electron wave function at the lth scatterer, which affects most severely on the scattering from the nearest neighbors. A detailed discussion of Eq. (4) can be found in Refs. 2, 6, and 13.

The dissipative nature of the incident beam in contributing to the observed Auger intensity complicates the calculation of the diffraction pattern. The intensity of the incident beam at the lth emitter, $I_{\text{in}}^{(l)}$, can be calculated by using Eq. (4) and substituting the relevant parameters for those of the incident beam.[6] We approximated the dissipation to the 0th order. That is, we took the derivative of the unscattered term in Eq. (4) with respect to z,

$$\frac{\partial}{\partial z_l} I_{\text{in,0th}}^{(l)} = \frac{\partial}{\partial z_l} \exp\left[-\frac{z_l / \cos\Theta_0}{\lambda_0}\right] = -\frac{1}{\lambda_0 \cos\Theta_0} I_{\text{in,0th}}^{(l)} , \tag{5}$$

and assumed that the dissipation of the incident beam in generating Auger electrons is mostly contained in the factor $1/\cos\Theta_0$. The contribution of the incident beam to the Auger intensity by exciting an Auger electron at the lth atom is therefore proportional to $I_{\text{in}}^{(l)}/\cos\Theta_0$, where $I_{\text{in}}^{(l)}$ is from Eq. (4), with appropriate replacement of the parameters. This 0th-order approximation of the incident-beam dissipation is parallel to the case in the continuum limit, presented in Eqs. (1) and (2). With these approximations, the total flux at the detector is given by

$$I(\Theta_0, \Theta_1, \Phi_0, \Phi_1) \propto \sum_l I_{\text{in}}^{(l)} I_{\text{out}}^{(l)} / \cos\Theta_0 , \tag{6}$$

where Φ_0 and Φ_1 are the azimuthal angles of the incident and exit beam, respectively.

In our calculations, we have selected a cluster size of $48 \times 57 \times 40$ Å^3 along $[1\bar{1}0]$, [001], and [110], respectively. The center atom of each layer parallel to the surface was chosen as the emitter based on the random-event argument for Auger excitation. The surface relaxation was modeled as having a constant bond length between the Ga and As as in the bulk with As atoms tilted outward 27°.[7,8] The mean free paths were chosen to be $\lambda_0 = 20$ Å and $\lambda_1 = 14$ Å. The scattering form factors $f(\theta)$ were taken from tabulated values based on free-atom scattering of incident plane waves for the outgoing Auger electrons.[14-16] For the incident beam, $f(\theta)$ was calculated using a muffin-tin potential with incident plane waves because the kinetic energy $E_0 = 3$ keV is beyond the range of the tables.[6] The calculated intensity is also convoluted over a small solid angle of 1×10^{-3} rad for comparison to the data taken with comparable angular resolution.

Comparison of data with single-scattering calculations

In Fig. 5, we compare the experimental data with single-scattering calculations for the incident polar-angle scan of Ga and As *LMM* emission from GaAs(110) along [001]. The data [Figs. 5(b) and 5(d)] were taken by simultaneously adjusting the sample and analyzer such that the exit angle Θ_1 was kept constant at −45°. The calculations [Figs. 5(a) and 5(c)] were carried out using Eq. (6) with parameters selected as described in the preceding section. All the curves were normalized to the maximum intensity, which is also done in the rest of the figures. Excellent agreement between the experimental data and calculated results, in terms of both the peak positions and heights, is clearly demonstrated. The calculated results have a slightly lower intensity for incident angle $\Theta_0 \geq 60°$, reflecting the inadequacy of the 0th-order approximation used in Eq. (6) for describing the dissipative nature of the incident beam.

The experimental and calculated exit polar-angle scans of the Ga and As *LMM* Auger intensities in GaAs(110) along [001] are presented in Fig. 6. The incident angle was kept at $\Theta_0 = 80°$. Again, the peak positions of the

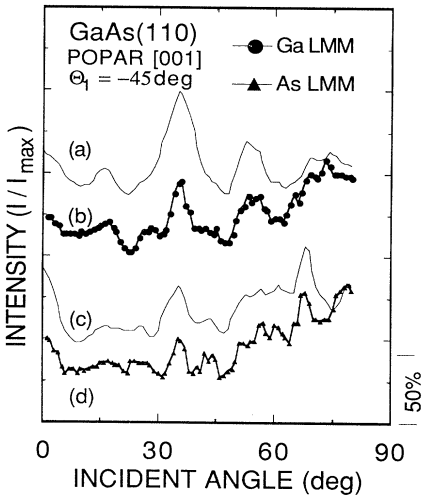

FIG. 5. Comparison of experimental data and theoretical curves for incident-beam polar-angle scan of Ga and As *LMM* Auger intensity from GaAs(110) along [001]. The exit angle was kept at $\Theta_1 = -45°$. (b) The theoretical curve for GA *LMM* using single-scattering calculations described by Eqs. (4)–(6); (b) experimental data for Ga *LMM*; (c) the theoretical curve for As *LMM*, using single-scattering calculations described by Eqs. (4)–(6); (d) experimental data for *LMM*.

calculated results [Figs. 6(b) and 6(d)] agree well with the experimental data [Figs. 6(a) and 6(b)]. The experimental data show a higher background, especially for smaller $|\Theta_1|$. We attribute the background to multiple scattering, which is known to reduce the forward-scattering intensity, resulting in a somewhat homogeneous background.[2,3,17,18] By comparing Figs. 5 and 6, it is evident that there is a sharp contrast in the richness of structures for larger polar angles, i.e., $|\Theta_i| > 60°$. We conclude that both incident and exit angular dependence can be described by single-scattering calculation. While the exit-angle dependence shows pronounced scattering features for $|\Theta_1| \leq 60°$ (Fig. 6), the incident-angle dependence adds more features at larger angles because of the $1/\cos\Theta_0$ factor. It is therefore demonstrated that the incident-angle polar scan has higher sensitivity at larger polar angles, which may consequently imply higher surface sensitivity resulted from the more glancing geometry. Another implication is that one can obtain higher signal intensity by preferentially selecting large incident angles in an electron-simulated Auger experiment.

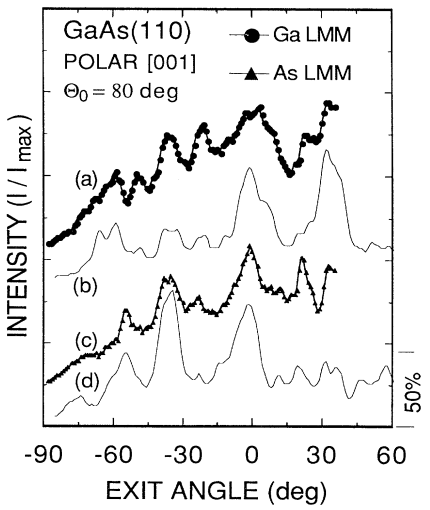

FIG. 6. A comparison of experimental data and theoretical curves for an exit-beam polar-angle scan of Ga and As *LMM* Auger intensity from GaAs(110) along [001]. The incident angle was kept at $\Theta_0 = 80°$. (a) Experimental data for Ga *LMM*; (b) the theoretical curve for Ga *LMM* using single-scattering calculations described by Eqs. (4)–(6); (c) experimental data of As *LMM*; (d) the theoretical curve for As *LMM*, using single-scattering calculations described by Eqs. (4)–(6).

Here we comment on previous observations that the incident-beam diffraction effects could be ignored. It may have been the consequence of a combination of the following reasons.

(i) An accidental coincidence of the peaks in incident-beam and exit-beam scattering in special cases. An example is having the scattering angle between the incident and exit beam fixed at $\Delta\Theta = \Theta_0 - \Theta_1 = 45°$, as is the case for some experimental setups,[6] and studying the polar-angle scan along [100] of the (001) surface of a cubic, bcc, or fcc crystal. In this case, the major scattering maximum at $\Theta_i = 0°$ and $|\Theta_i| = 45°$ will be simultaneous for both the incident and exit beams and, if one plots the scattering magnitude versus the exit angle Θ_1, the maximums at $\Theta_1 = 0°$ and $\Theta_1 = 45°$ will be enhanced relative to the case where there is no incident-beam scattering.

(ii) The dissipative nature of the incident beam in producing Auger transitions was not appreciated. From the qualitative picture presented in Eq. (3) and Figs. 3 and 4, and from the single-scattering calculations described by Eqs. (4)–(6) and shown in Figs. 5 and 6, we realize that although both incident beam and exit beam undergo the same forward-scattering mechanism, the polar-angle dependence of the two are different. Specifically, the dissipative nature of the incident-beam scattering emphasizes the large-polar-angle-scattering features, while the elastic-scattering of the exit beam favors smaller-polar-angle-scattering features. Consequently, if one does not include the incident-beam dissipation in calculating the scattering spectrum in a fixed analyzer–electron-gun angle experiment, a distortion will result and comparisons with experimental data may fail to show improvement over the one in which incident-beam effects are not included.

(iii) In some previous AED measurements, the data were normalized by dividing the background counts taken at a kinetic energy ~ 15 eV higher than that of the Auger signal.[6,19] This process removes the fluctuations of the electron gun, and at the same time it may also reduce the diffraction effects of the incident beam. In our experiments, such a normalization was not applied because the time for data acquisition was short enough and the electron-gun drifting was insignificant.

The points made above are further illustrated in Figs. 7 and 8. In Fig. 7 we show the data and calculation for Ga *LMM* Auger polar-angle scan from GaAs(110) along

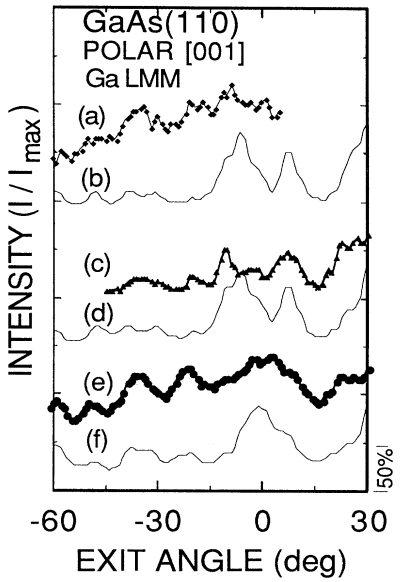

FIG. 7. The effects of incident-beam diffraction on the Ga *LMM* Auger intensity from GaAs(110) along [001]. (a) Experimental data taken with the angle between the incident and exit beams fixed at $\Delta\Theta=45°$; (b) the theoretical curve of the same geometry using single-scattering calculation described by Eqs. (4)–(6); (c) the convolution of the data shown in Figs. 3(a) and 4(a), with fixed $\Delta\Theta=45°$; (d) the convolution of the theoretical curves shown in Figs. 5(a) and 6(b), with fixed $\Delta\Theta=45°$; (e) experimental data on the exit-beam polar-angle dependence, reproduced from Fig. 6(a); (f) theoretical curve for the exit-beam polar-angle dependence, reproduced from Fig. 6(b).

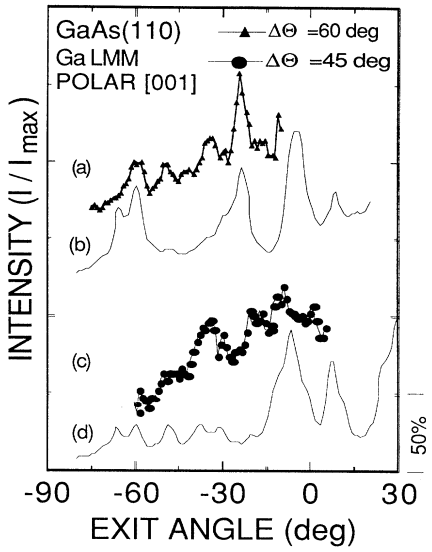

FIG. 8. The effects of a constant electron-gun–analyzer angle on the Ga *LMM* Auger intensity from GaAs(110) along [001]. (a) The experimental data taken with the angle between the incident and exit beams fixed at $\Delta\Theta=60°$; (b) the theoretical curve for the same geometry using the single-scattering calculation described by Eqs. (4)–(6); (c) experimental data taken with the angle between the incident and exit beams fixed at $\Delta\Theta=45°$; (d) theoretical curve for the same geometry, using the single-scattering calculation described by Eqs. (4)–(6). (c) and (d) are reproduced from Figs. 7(a) and 7(b).

[100]. Figure 7(a) shows the experimental data taken with the angle between the incident and exit beam fixed at $\Delta\Theta=45°$. Figure 7(b) shows the calculated results using Eq. (6), assuming the same geometry of $\Delta\Theta=45°$. Figure 7(c) is obtained by convoluting the data in Figs. 3 and 4 with $\Delta\Theta=45°$, and Fig. 7(d) is the convolution of the corresponding theoretical curves shown in Figs. 5 and 6. It is remarkable that Figs. 7(a) and 7(c) and Figs. 7(b) and 7(d) are essentially identical. In convoluting Fig. 7(d), we are, in fact, calculating

$$\left[\sum_l I_{\rm in}^{(l)} I_{\rm out}^{(l)} / \cos\Theta_0\right] \sum_m I_{\rm in}^{(m)} I_{\rm out}^{(m)} / \cos(80°)\Big|_{\Delta\Theta=45°},$$

which involves a lot of cross terms between emission from different layers. The agreement between Figs. 7(a) and 7(c) and between Figs. 7(b) and 7(d) reflects the quick convergence of emission from different layers resulting in the insignificance of the cross terms in generating new features. The general agreement between the experimental data and the calculations is good, with the exception of the peak at $\Theta_1=-10°$ in the data [Figs. 7(a) and 7(c)], which apparently corresponds to the peak in the theoretical curves [Figs. 7(b) and 7(d)] at $\Theta_1=-6°$. At the present time we can offer no explanation for this discrepancy. The significance of including incident-beam diffraction can be further illustrated by a comparison of the experimental and calculated results for the exit-beam polar-angle scans reproduced in Figs. 7(e) and 7(f), respectively. It can be seen that while the exit-beam polar-angle scan has a broad maximum centered at $\Theta_1=-2°$, resulting from the forward scattering in the [110] direction, the convoluted results, either from the fixed angle between incident- and exit-beam scan [Fig. 7(a)] or from independent incident-beam and exit-beam scan [Fig. 7(c)], have almost no peaks at the same position, instead having two peaks at $\Theta_1=-10°$ and 7°, respectively. Differences can also be observed in the other angular range. A similar behavior is also observed for As (data not shown). The results in Fig. 7 demonstrate conclusively that in AED experiments, both incident-beam and exit-beam diffraction are significant and one must incorporate both effects in analyzing the data.

One can anticipate that since incident-beam scattering plays an equally important role as exit-beam scattering in Auger-electron-diffraction experiments, the observed diffraction spectra will depend on $\Delta\Theta$, the angle between the incident and exit beam, if it is fixed. This anticipation is realized by our measurements performed at $\Delta\Theta=45°$ and 60°, shown in Fig. 8. Figure 8(a) is the Ga *LMM* Auger polar-angle scan along [001] of GaAs(110) with fixed $\Delta\Theta=60°$, and Fig 8(c) is the scan with $\Delta\Theta=45°$, reproduced from Fig. 7(a). Figures 8(b) and 8(d) are corresponding theoretical curves calculated with use of Eq. (6). The difference between the two sets of curves is obvious. The most pronounced is the sharp peak at

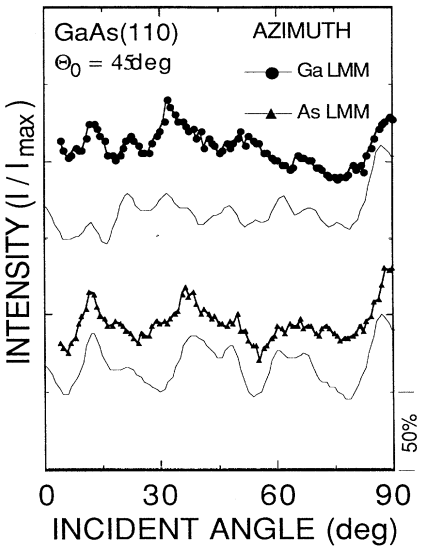

FIG. 9. A comparison of experimental data and theoretical curves for the incident-beam azimuthal-angle scan of Ga and As *LMM* Auger intensity from GaAs(110). The incident-beam polar angle was kept at $\Theta_0=45°$ and the exit-beam polar angle was kept at $\Theta_1=0°$. (a) Experimental data for Ga *LMM*; (b) the theoretical curve for Ga *LMM*, using the single-scattering calculations described by Eqs. (4)–(6); (c) experimental data for As *LMM*; (d) the theoretical curve for As *LMM*, using the single-scattering calculations described by Eqs. (4)–(6).

$\Theta_1=-24°$, present in both the experimental data [Fig. 8(a)] and the theoretical curve [Fig. 8(b)] for $\Delta\Theta=60°$. At the same position the $\Delta\Theta=45°$ curves [Figs. 8(c) and 8(d)] are at a minimum. These results strongly suggest that one has to exercise great care when comparing AED data taken with different spectrometers that have different fixed angles between the analyzer and electron gun.

The results in Fig. 5 demonstrate that the 0th-order approximation Eq. (6) can account reasonably well for the dissipative nature of the incident-beam scattering. With this approximation we can also speculate that in the case of azimuthal-angle scans differences between the incident-angle scan and exit-angle scan will diminish since they differ mostly by a constant factor $1/\cos\Theta_0$. This speculation was verified by data from incident-beam azimuthal-angle scans shown in Figs. 9(a) and 9(c), together with the results of single-scattering calculations using Eq. (6) [Figs. 9(b) and 9(d)]. The azimuthal-angle scans were taken with polar angles $\Theta_0=45°$ and $\Theta_1=0°$, respectively, which results in constant scattering angles for the outgoing Auger electrons throughout the scan. Again, the agreement between the calculation and the experimental data suggests that most of the diffraction features are contained in $I_{\rm in}^{(l)}$ and that the 0th-order approximation of the incident-beam dissipation, used in Eq. (6), is adequate for describing the incident-beam scattering. We conclude that while the polar-angle scans show the fundamental difference between incident- and exit-beam scattering, especially at glancing angles, in the azimuthal-angle scans the difference between the two types of scans is not as significant.

CONCLUSIONS

We have designed and performed experiments to examine critically the diffraction effects of the incident beam in electron-stimulated Auger-electron diffraction and our results indicate that incident-beam diffraction is significant and must be considered, in general, in examining AED data. The dissipative nature of the incident beam in generating Auger electrons causes an enhancement of scattering features at large polar angles, which is complementary to that for the exit-beam polar-angle scan. We have developed a qualitative model in the continuum limit which explains well the trend of the polar-angle dependence of both the incident and exit beams. We have derived a 0th-order approximation for calculating the diffraction features. A comparison with the experimental data suggests that the approximation is adequate, and that the incident-beam diffraction effects are mostly contained in the elastic part of the scattering.

ACKNOWLEDGMENTS

This work was supported in part by the National Science Foundation under Grant No. DMR-89-3880. One of us (Y.G.) gratefully acknowledges partial support from the Alfred P. Sloan Foundation. The authors are indebted to S. A. Chambers, who has also generously supplied part of the computer code for the calculations, for stimulating interactions. Some technical assistance from Ken T. Park is also acknowledged.

[1]S. A. Chambers, T. R. Greenlee, C. P. Smith, and J. H. Weaver, Phys. Rev. B **32**, 4245 (1985).
[2]C. S. Fadley, in *Synchrotron Radiation Research Advances in Surface and Interface Science,* edited by R. Z. Bachrack (Plenum, New York, 1990).
[3]W. F. Egelhoff, Jr., Crit. Rev. Solid State Mater. Sci. **16**, 213 (1990).
[4]H. C. Poon and S. Y. Tong, Phys. Rev. B **30**, 6211 (1984).
[5]C. S. Fadley, in *Progress in Surface Science,* edited by S. G. Davison (Pergamon, New York, 1984), Vol. 16, p. 275.
[6]S. A. Chambers, I. M. Vitomiron, and J. H. Weaver, Phys. Rev. B **36**, 3007 (1987).
[7]S. Y. Tong, A. R. Lubinsky, B. J. Mrstik, and M. A. Van Hove, Phys. Rev. B **17**, 3303 (1978).
[8]C. B. Duke and A. Paton, Surf. Sci. **164**, L797 (1985).
[9]S. M. Sze, in *Physics of Semiconductor Devices,* 2nd ed. (Wiley, New York, 1981).
[10]J. W. Gadzwk, Surf. Sci. **60**, 76 (1976).
[11]T. N. Rhodin and J. W. Gadzwk, in *The Nature of the Surface Chemical Bond,* edited by T. N. Rhodin and G. Ertl (North-Holland, Amsterdam, 1979), p. 115.
[12]M. P. Seah and W. A. Dench, Surf. Interf. Anal. **1**, 2 (1979).

[13]H. C. Poon, D. Snider, and S. Y. Tong, Phys. Rev. B **33**, 2198 (1988).
[14]M. Fink and J. Ingram, At. Data **4**, 129 (1972).
[15]D. Gregory and M. Fink, At. Data Nucl. Data Tables **14**, 39 (1974).
[16]We have also tried using a muffin-tin-potential scattering factor to calculate AED for outgoing waves. The results show no significant difference from those obtained with the use of the tabulated one.
[17]S. Y. Tong, H. C. Poon, and D. R. Snider, Phys. Rev. B **32**, 2096 (1985).
[18]M. L. Xu, J. J. Barton, and M. A. Van Hove, Phys. Rev. B **39**, 8275 (1989).
[19]S. A. Chambers, G. A. Howell, T. R. Greenlee, and J. H. Weaver, Phys. Rev. B **31**, 6402 (1985).